

Phonon softening and crystallographic orientation of strained graphene studied by Raman spectroscopy

Mingyuan Huang^{a,1}, Hugen Yan^{b,1}, Changyao Chen^a, Daohua Song^b, Tony F. Heinz^b, and James Hone^{a,2}

^aDepartment of Mechanical Engineering, Columbia University, New York, NY 10027; and ^bDepartments of Physics and Electrical Engineering, Columbia University, New York, NY 10027

Edited by Mildred S. Dresselhaus, Massachusetts Institute of Technology, Cambridge, MA, and approved March 9, 2009 (received for review November 18, 2008)

We present a systematic study of the Raman spectra of optical phonons in graphene monolayers under tunable uniaxial tensile stress. Both the G and 2D bands exhibit significant red shifts. The G band splits into 2 distinct subbands (G⁺, G⁻) because of the strain-induced symmetry breaking. Raman scattering from the G⁺ and G⁻ bands shows a distinctive polarization dependence that reflects the angle between the axis of the stress and the underlying graphene crystal axes. Polarized Raman spectroscopy therefore constitutes a purely optical method for the determination of the crystallographic orientation of graphene.

Since the discovery of mechanical cleavage of graphene from graphite crystals (1), graphene has attracted intense interest because of properties that include high electron mobility (2, 3), novel quantum Hall physics (4, 5), superior thermal conductivity (6), and unusually high mechanical strength (7). Raman spectroscopy has emerged as a key diagnostic tool to identify single-layer graphene sheets (8) and probe their physical properties (9, 10). Because strain induces shifts in the vibrational frequencies, Raman spectroscopy can be applied to map built-in strain fields during synthesis (11) and device fabrication, as well as measure load transfer in composites. The rate of shift of the phonon frequencies with strain depends on the anharmonicity of the interatomic potentials of the atoms in the honeycomb lattice and thus can be used to verify theoretical models.

Measurement of the strain dependence of the Raman active phonons is thus important for both applied and fundamental studies of this material system (12). By using graphene supported on a flexible substrate, we have been able to obtain precise information on the rate of frequency shift of the Raman G (zone-center optical) and 2D (two-phonon zone-edge optical) modes with strain. In addition, the polarization dependence of the Raman response in strained graphene can, as we demonstrate in this article, be used for an accurate determination of the crystallographic orientation. For unstrained graphene, such an orientation analysis is precluded by the high symmetry of the hexagonal lattice. A particularly important application of this capability lies in the study of nanopatterned graphene monolayers, such as nanoribbons (13) and quantum dots (14). Graphene nanoribbons possess electronic band gaps whose magnitude reflects both the ribbon width and crystallographic orientation (13, 15–17). The electronic states associated with graphene edges are also sensitive to the crystallographic orientation of the ribbon (18). It is thus crucial to be able to correlate the measured properties to the underlying crystallographic orientation of the sample. As we show here, polarized Raman spectroscopy provides a simple, but precise analytic tool that complements electron-spectroscopy techniques such as scanning tunneling microscopy (STM) (19), transmission electron microscopy (TEM) (20), and low-energy electron diffraction (LEED) (21), methods that typically require ultrahigh vacuum conditions and specialized equipment.

Results and Discussion

Phonon Softening. Fig. 1 *A* and *B* show the 2D and G bands of graphene under increasing strain. As expected, both bands

exhibit significant red shifts. Further, the G mode peak splits as the graphene symmetry is lowered by the strain. Unstrained graphene belongs to the 2D point group D_6 and displays C_6 and m symmetry. Under strain only C_2 symmetry will generally be retained. (If the strain is in the armchair or zigzag direction, m symmetry will also survive.) Therefore, the G band, which results from a doubly degenerate optical phonon mode with E_{2g} symmetry, splits into 2 singlet bands, which we denote by G^+ and G^- , according to their energy. Fig. 1C shows the positions of the 2D, G^+ , and G^- peaks versus applied strain. All 3 modes shift linearly with strain, with shift rates of -21 ± 4.2 , -12.5 ± 2.6 , and -5.6 ± 1.2 $\text{cm}^{-1}/\%$ for the 2D, G^- , and G^+ bands, respectively [the uncertainty is dominated by the systematic uncertainty in strain calibration; see [supporting information \(SI Text\)](#)]. In recent experiments over a smaller strain range, Ni et al. (12) found a similar shift rate for the 2D mode. However, the strain-induced splitting and polarization dependence of the graphene G mode have not been previously observed. Therefore, below we focus exclusively on the G mode.

The G band of graphene is a long wavelength ($q = 0$) optical phonon mode in which the 2 sublattices vibrate with respect to each other. A phenomenological method can be used to analyze the Raman modes in the presence of strain (22). Following the standard procedure (see [SI Text](#)), we can write the secular equation for the G band of strained graphene as

$$\begin{vmatrix} A\varepsilon_{xx} + B\varepsilon_{yy} - \lambda & (A - B)\varepsilon_{xy} \\ (A - B)\varepsilon_{xy} & B\varepsilon_{xx} + A\varepsilon_{yy} - \lambda \end{vmatrix} = 0 \quad [1]$$

where $\lambda \equiv \omega^2 - \omega_0^2$ is the difference between the square of the perturbed and unperturbed phonon frequencies, A and B are the phonon deformation potential coefficients, and ε_{ij} is the strain tensor. Because second- and fourth-order tensors describing the in-plane response of the hexagonally symmetric graphene have the same form as those of isotropic materials, the secular equation holds in any coordinate system in the graphene plane. In the experimental coordinate system, the strain tensor can be reduced to $\varepsilon_{xx} = \varepsilon$, $\varepsilon_{yy} = -\nu\varepsilon$, and $\varepsilon_{xy} = 0$, where x is the direction of the applied stress, ε is the magnitude of the resulting strain, and $\nu = 0.16$ is the Poisson ratio (23). The transverse strain described by the Poisson ratio is expected for the unconstrained lateral boundaries of the

Author contributions: M.H., H.Y., T.F.H., and J.H. designed research; M.H., H.Y., and C.C. performed research; M.H., H.Y., D.S., T.F.H., and J.H. analyzed data; and M.H., H.Y., T.F.H., and J.H. wrote the paper.

The authors declare no conflict of interest.

This article is a PNAS Direct Submission.

¹M.H. and H.Y. contributed equally to this work.

²To whom correspondence should be addressed. E-mail: jh2228@columbia.edu.

This article contains supporting information online at www.pnas.org/cgi/content/full/0811754106/DCSupplemental.

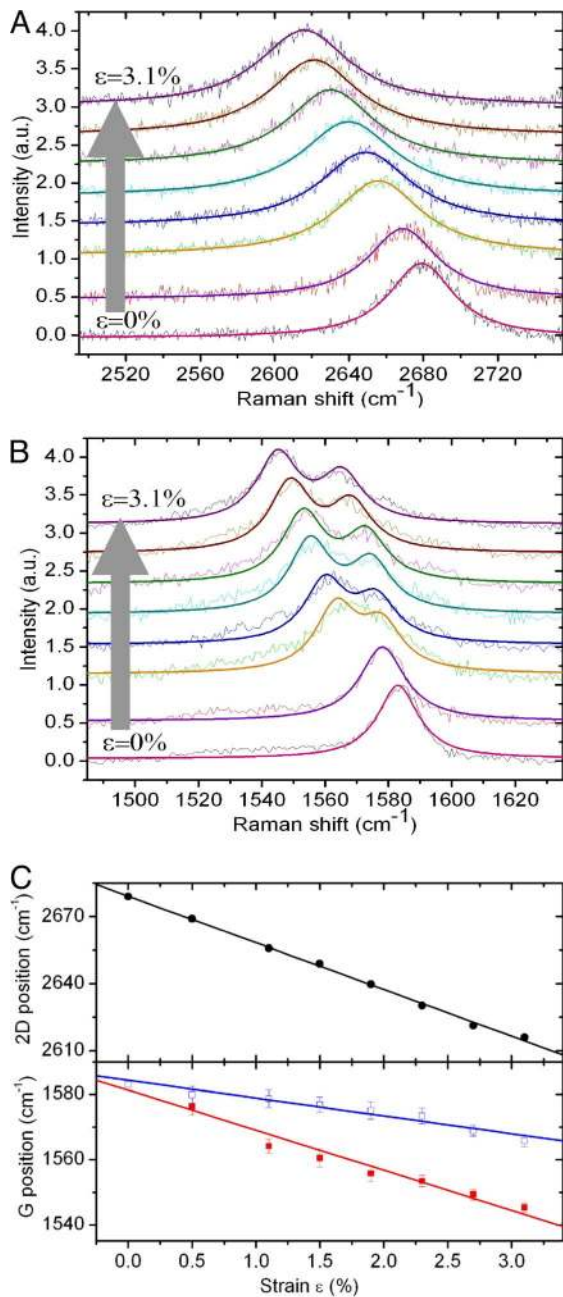


Fig. 1. Strain-induced phonon softening in graphene. (A, B) Evolution of the spectra of the 2D (A) and G (B) bands of graphene under strain. The spectra of the 2D band and the first 2 spectra of the G band are fit by single Lorentz peaks; the other G band spectra are fit by 2 Lorentz peaks of fixed width 16 cm^{-1} (smooth overlapping curves), as extracted from the polarization study shown below (Fig. 3B). The difference between the G band data and the fits is attributed to scattering from the PDMS substrate. (C) The variation of the phonon frequencies of 2D, G^+ and G^- bands from A and B as a function of strain. The solid lines are linear fits.

graphene strip under uniaxial stress (see *SI Text*). We then find that the frequencies of the G^+ and G^- modes are given by

$$\begin{cases} \omega_{G^+} = \omega_0 + \frac{B - vA}{2\omega_0} \varepsilon \\ \omega_{G^-} = \omega_0 + \frac{A - vB}{2\omega_0} \varepsilon \end{cases} \quad [2]$$

The corresponding eigenvectors for the atomic displacements are perpendicular to the direction of stress for the G^+ mode, and parallel for the G^- mode.

Using the measured shift rates, we find for the phonon deformation potential coefficients $A = -4.4 \pm 0.8 \times 10^6 \text{ cm}^{-2}$ and $B = -2.5 \pm 0.5 \times 10^6 \text{ cm}^{-2}$ of the G band. To compare the results with previous experiments on graphite performed under 3D hydrostatic pressure, we use the values of A and B, and the effective in-plane Young's modulus, to calculate the shift rate of graphene under 2D hydrostatic pressure. The inferred shift rate is $1.9 \pm 0.4 \text{ cm}^{-1}/\text{GPa}$, smaller than the value measured from graphite ($4.6 \text{ cm}^{-1}/\text{GPa}$) (24). The larger value for graphite may reflect its interlayer interactions, which are strongly altered by pressure: the shear mode frequency, for example, increases $\approx 100\%$ under 14 GPa. From the phonon deformation potential coefficients, the resulting G mode Grüneisen constant and shear phonon deformation potential (SDP) are 0.69 ± 0.14 and 0.38 ± 0.08 , respectively. Recent theoretical calculations (25) yield values for both parameters (Grüneisen constant, 2.0; SDP, 0.66) that exceed the measurements by more than the experimental uncertainty. The reason for the discrepancy is unclear at this point.

Determination of the Crystallographic Orientation. Polarized Raman spectroscopy can give insight into crystal orientation and vibrational symmetry. We have studied the polarization of the G^+ and G^- bands with the incident light polarized parallel to the principal strain axis. Fig. 2 A and B present 2D plots of the Raman intensity as a function of Raman shift and angle ϕ between the incident and scattered light polarization for 2 different graphene samples. Both the G^+ and G^- bands exhibit strong polarization dependence. This stands in contrast to the isotropic Raman response of the G band for unstrained graphene. For sample 1 (Fig. 2A), the G^+ band intensity peaks for the analyzer set near $\phi = 75^\circ$ and nearly vanishes for $\phi = 165^\circ$. The polarization of the scattered Raman radiation in the G^- band is simply shifted by 90° . The results of sample 2 (Fig. 2B) are similar, but with the maxima occurring at different angles. These findings indicate that the scattered light polarization is affected by the crystal orientation. To quantify the polarization properties of the Raman scattering process for G^+ and G^- bands, their intensity is plotted in Fig. 2 C and D as a function of the angle of the analyzer. The polarization dependence can be fit by the form $\sin^2(\phi - \phi_0)$ with $\phi_0 = 165.3^\circ, 75.8^\circ$ for the G^+ and G^- modes, respectively, for sample 1, and with $\phi_0 = 53.6^\circ, 140^\circ$ for sample 2. This indicates that the scattered light from G^+ and G^- bands is linearly polarized, and that the 2 modes have orthogonal polarizations.

According to the usual semiclassical treatment, first-order Raman scattering arises from the derivative of the electric susceptibility with respect to the atomic displacement of the relevant vibration. The polarization dependence of the scattering intensity can then be expressed as $I_s \propto |\mathbf{e}_i \mathbf{R} \mathbf{e}_s|^2$ (26), where \mathbf{e}_i and \mathbf{e}_s are the unit vectors describing the polarizations of the incident and scattered light. The Raman tensor \mathbf{R} is determined by the symmetries of crystal and vibrational mode. The G mode of unstrained graphene is doubly degenerate. Two Raman tensors (in the crystal reference system indicated in Fig. 2F) contribute to the total scattering intensity:

$$R_x = \begin{bmatrix} 0 & d \\ d & 0 \end{bmatrix} \quad R_y = \begin{bmatrix} d & 0 \\ 0 & -d \end{bmatrix} \quad [3]$$

Here, R_x and R_y correspond to the modes in which carbon atoms vibrate along the lattice x and y directions. These modes scatter light in such a way that the polarization vector is reflected, respectively, about the lines $x = y$ and $y = 0$. Because the scattering intensities are equal for the 2 modes, this process

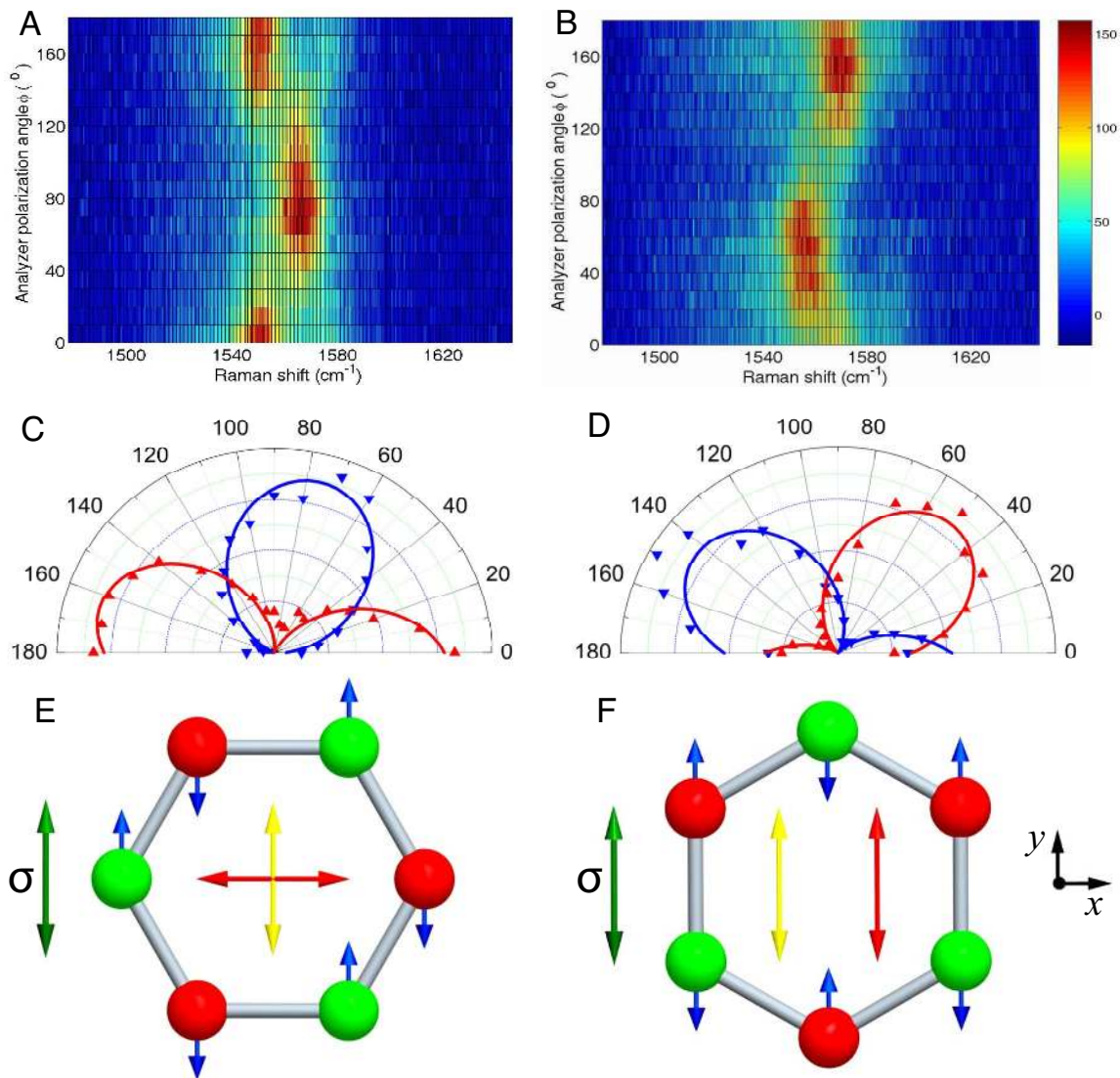


Fig. 2. Polarization analysis of the G band of strained graphene. (A, B) False-color image of the intensity of the Raman scattered light as a function of the Raman shift and angle of the analyzer ϕ for detection of the Raman signal. The angle ϕ was measured with respect to the incident light polarization, which was aligned along the strain axis. The data were obtained by measuring Raman spectra every 10° for sample 1 ($\epsilon = 2.3\%$, A) and 2 ($\epsilon = 1.9\%$, B). (C, D) Raman scattering intensity for the G^+ (blue triangle) and G^- (red triangle) bands as a function of ϕ for samples 1 and 2, respectively. The solid lines are fits to the form of $\sin^2(\phi - \phi_0)$. (E, F) Schematic representation of the vibrational modes for the G^- bands when the strain axis (green arrow) is, respectively, in the zigzag (E) and the armchair (F) directions of the graphene crystal. The yellow arrows represent the polarization of the incident light, which is chosen as parallel to the strain axis. The red arrows show the resulting polarization of the Raman scattered light for the G^- mode. The coordinate system in F represents the crystal reference system.

completely depolarizes the inelastically scattered light, rendering the G band response independent of polarization.

As discussed above, strain splits the G band into G^- and G^+ bands whose normal modes are parallel and perpendicular to the strain axis, respectively. The polarization of the scattered light from each mode will then depend on the direction of the strain relative to the crystal lattice. Consider, for example, 2 cases in which the incident light is polarized parallel to the strain. If the strain is in the “zigzag” direction (Fig. 2E), the G^- mode is equivalent to R_x , and the scattered light is polarized perpendicular to the strain direction. If the strain is in the “armchair” direction (Fig. 2F), the G^- mode is equivalent to R_y , and the scattered light is polarized parallel to the strain direction. Conversely, the G^+ band corresponds to R_y for strain along the zigzag axis and to R_x for strain along the armchair axis, leading to polarization perpendicular to that of the G^- mode.

For quantitative analysis of the polarization, we consider a general case in which the strain is at an arbitrary angle θ with

respect to the graphene crystallographic x axis. The Raman tensors of the G^+ and G^- bands are given by linear combinations: $R^\pm = v_x^\pm R_x + v_y^\pm R_y$, where (v_x^+, v_y^+) , (v_x^-, v_y^-) are, respectively, unit vectors along the direction of vibration of the G^+ and G^- bands. We denote by the angles ψ , ϕ the orientation with respect to the strain axis of the incident and scattered polarization vectors \mathbf{e}_i , \mathbf{e}_s in the Raman process. We then predict (see *SI Text* and Fig. S1 for details) that the intensities of the G^+ and G^- bands will then vary as

$$\begin{cases} I_{G^+} & \propto d^2 \cos^2(\phi + \psi + 3\theta) \\ I_{G^-} & \propto d^2 \sin^2(\phi + \psi + 3\theta) \end{cases} \quad [4]$$

This result is consistent with the experimental observation that the G^+ and G^- bands produce linearly polarized radiation with orthogonal polarization states. In addition, Eq. 4 shows that the polarization of the Raman scattered light is determined by the

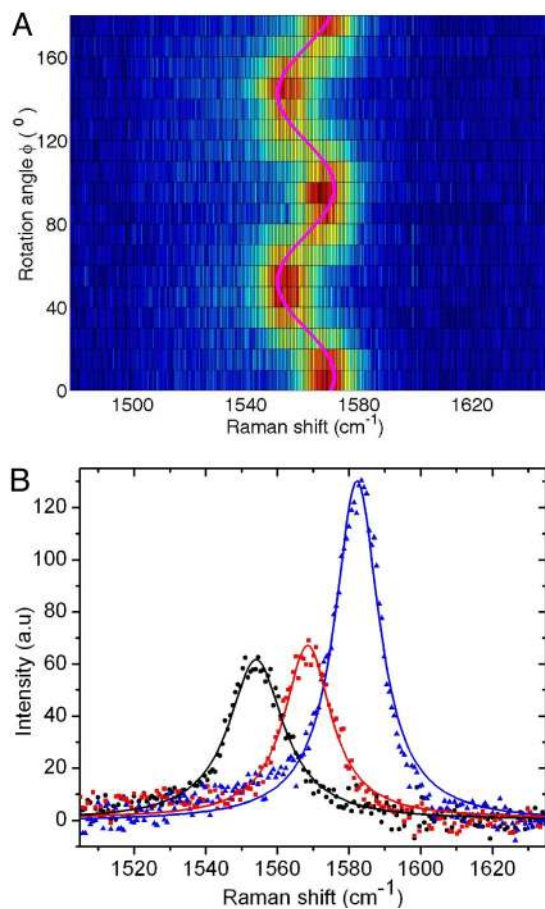


Fig. 3. The dependence of Raman spectra on the sample orientation. (A) False color image of the Raman intensity as a function of the Raman shift and the angle ϕ of rotation of the strained graphene sample ($\epsilon = 2.3\%$) about its surface normal. The magenta curve, which acts as a guide to the eye, is the intensity of the G^- or G^+ bands (measured to the left and right, respectively). The polarizations of the pump radiation and detected Raman radiation were fixed and perpendicular to one another. (B) Comparison of the spectra of the pure G^- , G^+ , and G bands. The spectra of the G^- (black circles, obtained for $\phi = 50^\circ$) and G^+ (red squares, obtained for $\phi = 0^\circ$) are included in A, and the spectrum of the G mode (blue triangles) was measured on the same sample without strain. The fits (solid lines) are Lorentzian in shape.

angle between the strain axis and the graphene crystal axes (with $\psi = 0$ for the experimental conditions). Analysis of the polarization dependence of the Raman scattering process thus provides an optical method of determining the orientation of the graphene crystallographic axes. Comparing our experimental results with Eq. 4, we conclude that for sample 1 the strain is applied at an angle of $25.2 \pm 0.1^\circ$ from the zigzag direction, whereas for sample 2 the strain is applied at $12.7 \pm 0.6^\circ$ from the zigzag direction.

To further confirm the theoretical analysis, an additional measurement was performed. We rotated sample 1 about its surface normal, whereas the incident and detected light polarizations remained fixed and perpendicular to one another. The data (Fig. 3A) show that the period of variation in the scattering intensity from each band is 90° . This result is consistent with Eq. 4, because rotation of the sample is equivalent to a simultaneous and equal change of ψ and ϕ . The maximal intensities of the G^+ and G^- bands (Fig. 3B) are equal to one another, and approximately half of the G band intensity measured without a polarizer. This behavior is consistent with the Raman tensor analysis above and indicates that the strain does not significantly change the strength of the Raman scattering process.

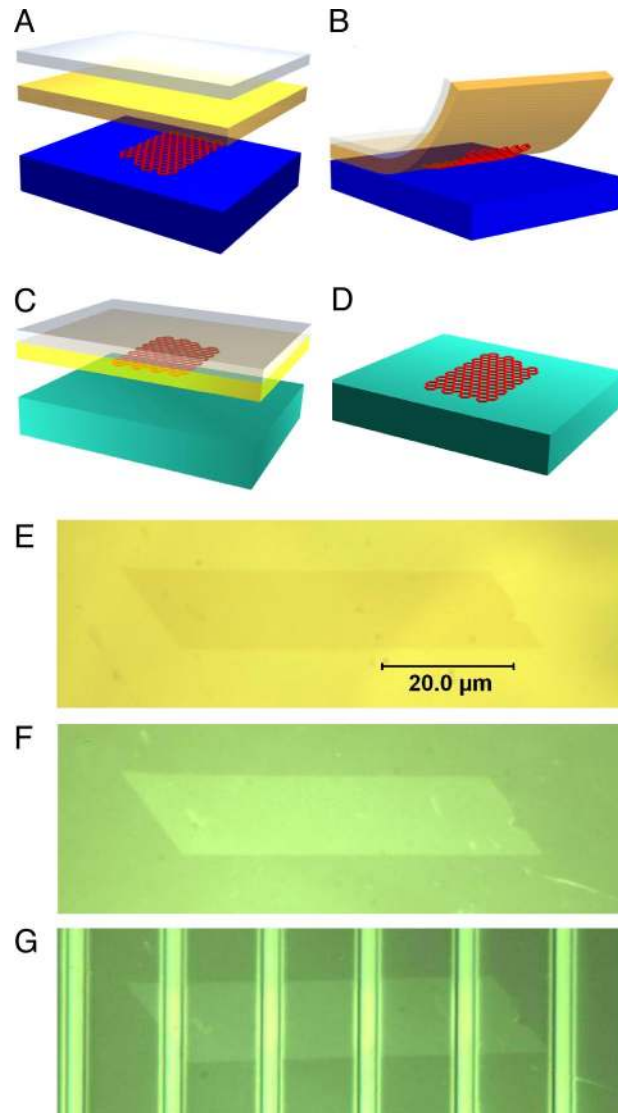


Fig. 4. Graphene transfer process. (A–D) Schematic illustration of the transfer of graphene from Si wafer to the PDMS film. The initial step involved deposition of a gold film (yellow) on the Si wafer supporting graphene monolayer; concentrated polyvinyl alcohol (PVA) solution was then cast onto the gold film (A). After the PVA solidified, it was peeled off from the Si wafer, carrying with it the gold and graphene films (B), which were then transferred onto PDMS substrate (C). In the last step, the PVA was washed away by DI water and the gold was dissolved by etching (D). (E–G) The same graphene on the Si wafer (before transfer) (E), on the PDMS substrate (after transfer) (F), and as clamped by Ti strips (G).

Finally, we note that both the G^+ and G^- bands have the same spectral width as that of the G band without applied strain. This finding implies that the strain within the laser spot ($\approx 1 \mu\text{m}$) is very homogeneous, consistent with the results of finite-element simulation (see *SI Text* and Fig. S2). It also indicates that the electron-phonon coupling strength, which largely defines the linewidth, is equivalent for G^+ and G^- phonons. The last result stands in contrast to the case of metallic carbon nanotubes, whose G^+ and G^- modes exhibit distinct coupling to electron-hole pair excitations (10, 27). This difference arises from the 1D structure of nanotubes, which acts to enhance the LO phonon interaction with electrons (28).

An important potential application of this technique involves the fabrication of graphene nanoribbons and similar devices that

are oriented along a predetermined crystal axis. For these applications, one would like to determine the lattice orientation directly on a Si wafer without transferring the graphene sample to a flexible substrate. From Fig. 1*B*, we observe that at least 1.5% strain is needed to separate G^+ and G^- bands fully from one another. However, such a complete separation of the peaks is not necessary for determining the crystal orientation: For smaller strains, the apparent position of the G band will vary with the detected Raman polarization. Assuming that a modulation of $\approx 2 \text{ cm}^{-1}$ can be observed, the crystal orientation could then be measured with an applied strain of $\approx 0.3\%$, which can be achieved on Si substrates (29).

Conclusion

In summary, we have transferred monolayer graphene onto flexible substrates and measured the Raman spectrum under uniaxial tensile strain. The 2D and G bands exhibit red shifts and the G band splits into 2 distinct (G^+ , G^-) features because of the strain-induced breaking of the crystal symmetry. Unlike for the G mode of unstrained graphene, Raman scattering from the G^+ and G^- modes exhibits strong polarization dependence, with a response that depends on the orientation of the graphene crystal lattice. This behavior permits a precise determination of the crystallographic orientation of graphene monolayers by means of a purely optical technique.

Materials and Methods

Sample Fabrication. The graphene samples investigated in this study were prepared by mechanical exfoliation of kish graphite (1). Monolayer flakes,

deposited on Si wafers with a 290-nm SiO_2 epilayer, were initially identified by optical microscopy and their nature was confirmed by Raman spectroscopy (8). After a suitable graphene flake was selected, we transferred the graphene monolayer from the Si wafer onto the surface of a polydimethylsiloxane (PDMS) film, a clear silicone elastomer suitable for the application of stress. The transfer technique, outlined in Fig. 4 *A–D*, is similar to that previously demonstrated for carbon nanotubes (30). Fig. 4 *E* and *F* show optical images of a graphene flake on the SiO_2 surface (before transfer) and on the PDMS film (after transfer). We note that this method can be used to transfer graphene from the Si/SiO_2 substrate, where it is particularly easy to identify, to any other substrate. The graphene monolayer is still visible on the transparent PDMS substrate, a result that can be confirmed by a reflectance calculation (31). To clamp the graphene onto the PDMS film after its transfer, we patterned narrow strips of titanium (60 nm thick, $2 \mu\text{m}$ wide) on the samples by evaporation through a shadow mask (Fig. 4*G*).

Raman Spectroscopy. Uniaxial stress was applied to the graphene in a direction perpendicular to the Ti strips by controlled bending of the PDMS. The induced longitudinal strain was determined directly by measuring the distance between the strips in an optical microscope. For the transverse direction, the strain was calculated from the Poisson ratio (see *SI Text*). The applied strain was completely reversible, indicating that there was no slippage or permanent modification of the sample when stressed. For Raman spectroscopy, a 532-nm excitation laser was focused on the graphene monolayer by a $40\times$ microscope objective with a N.A. of 0.52. The Raman shifted light was collected by the same objective in a backscattering configuration. The laser power was kept sufficiently low ($<1 \text{ mW}$) to avoid heating during the measurement.

ACKNOWLEDGMENTS. This work was supported by the Nanoscale Science and Engineering Initiative of the National Science Foundation (Nanoscale Interdisciplinary Research Teams Grant ECS-05-07111), the Defense Advanced Research Planning Agency Center on Nanoscale Science and Technology for Integrated Micro/Nano-Electromechanical Transducers (Grant HR0011-06-1-0048).

- Novoselov KS, et al. (2004) Electric field effect in atomically thin carbon films. *Science* 306:666–669.
- Bolotin KI, et al. (2008) Ultrahigh electron mobility in suspended graphene. *Solid State Commun* 146:351–355.
- Du X, Skachko I, Barker A, Andrei EY (2008) Approaching ballistic transport in suspended graphene. *Nat Nanotechnol* 3:491–495.
- Zhang YB, Tan YW, Stormer HL, Kim P (2005) Experimental observation of the quantum Hall effect and Berry's phase in graphene. *Nature* 438:201–204.
- Novoselov KS, et al. (2005) Two-dimensional gas of massless Dirac fermions in graphene. *Nature* 438:197–200.
- Balandin AA, et al. (2008) Superior thermal conductivity of single-layer graphene. *Nano Lett* 8:902–907.
- Lee C, Wei X, Kysar JW, Hone J (2008) Measurement of the elastic properties and intrinsic strength of monolayer graphene. *Science* 321:385–388.
- Ferrari AC, et al. (2006) Raman spectrum of graphene and graphene layers. *Phys Rev Lett* 97:187401.
- Pisana S, et al. (2007) Breakdown of the adiabatic Born-Oppenheimer approximation in graphene. *Nat Mater* 6:198–201.
- Yan J, Zhang YB, Kim P, Pinczuk A (2007) Electric field effect tuning of electron-phonon coupling in graphene. *Phys Rev Lett* 98:166802–166805.
- Ferralis N, Maboudian R, Carraro C (2008) Evidence of Structural Strain in Epitaxial Graphene Layers on 6H-SiC(0001). *Phys Rev Lett* 101:156801.
- Ni ZH, et al. (2008) Uniaxial strain on graphene: Raman spectroscopy study and band-gap opening. *ACS Nano* 2:2301–2305.
- Han MY, Ozyilmaz B, Zhang YB, Kim P (2007) Energy band-gap engineering of graphene nanoribbons. *Phys Rev Lett* 98:206805.
- Ponomarenko LA, et al. (2008) Chaotic dirac billiard in graphene quantum dots. *Science* 320:356–358.
- Son YW, Cohen ML, Louie SG (2006) Energy gaps in graphene nanoribbons. *Phys Rev Lett* 97:216803.
- Barone V, Hod O, Scuseria GE (2006) Electronic structure and stability of semiconducting graphene nanoribbons. *Nano Lett* 6:2748–2754.
- Wang XR, et al. (2008) Room-temperature all-semiconducting sub-10-nm graphene nanoribbon field-effect transistors. *Phys Rev Lett* 100:206803.
- Nakada K, Fujita M, Dresselhaus G, Dresselhaus MS (1996) Edge state in graphene ribbons: Nanometer size effect and edge shape dependence. *Phys Rev B* 54:17954–17961.
- Stolyarova E, et al. (2007) High-resolution scanning tunneling microscopy imaging of mesoscopic graphene sheets on an insulating surface. *Proc Natl Acad Sci USA* 104:9209–9212.
- Meyer JC, et al. (2007) The structure of suspended graphene sheets. *Nature* 446:60–63.
- Knox KR, et al. (2008) Spectromicroscopy of single and multilayer graphene supported by a weakly interacting substrate. *Phys Rev B* 78:201408R.
- Ganesan S, Maradudi AA, Oitmaa J (1970) A lattice theory of morphic effects in crystals of diamond structure. *Ann Phys* 56:556–594.
- Kelly BT (1981) *Physics of Graphite* (Applied Science Publishers, London), p 477.
- Hanfland M, Beister H, Syassen K (1989) Graphite under pressure—Equation of state and 1st-order Raman modes. *Phys Rev B* 39:12598–12603.
- Thomsen C, Reich S, Ordejon P (2002) Ab initio determination of the phonon deformation potentials of graphene. *Phys Rev B* 65:073403.
- Loudon R (1964) Raman effect in crystals. *Adv Phys* 13:423–482.
- Wu Y, et al. (2007) Variable electron-phonon coupling in isolated metallic carbon nanotubes observed by Raman scattering. *Phys Rev Lett* 99:027402.
- Piscanec S, Lazzeri M, Robertson J, Ferrari AC, Mauri F (2007) Optical phonons in carbon nanotubes: Kohn anomalies, Peier's distortions, and dynamic effects. *Phys Rev B* 75:035427.
- Son H, et al. (2007) Strain and friction induced by van der Waals interaction in individual single walled carbon nanotubes. *Appl Phys Lett* 90:253113.
- Meitl MA, et al. (2006) Transfer printing by kinetic control of adhesion to an elastomeric stamp. *Nat Mater* 5:33–38.
- Blake P, et al. (2007) Making graphene visible. *Appl Phys Lett* 91:063124.